JAERI-M
92-173

DYNAMIC BEHAVIORS OF FRAGMENTS EJECTED FROM THE SURFACE OF CARBON MATERIALS BY LASER ABLATION

October 1992

Osamu YODA, Atsumi MIYASHITA, Takasumi OHYANAGI*
and Kouichi MURAKAMI*

日本原子力研究所
Japan Atomic Energy Research Institute

JAERI-Mレポートは，日本原子力研究所が不定期に公刊している研究報告書です。
入手の問合わせは，日本原子力研究所技術情報部情報資料課（〒319-11茨城県那珂郡東海村）あて，お申しこしください。なお，このほかに財団法人原子力弘済会資料センター（〒319-11 茨城県那珂郡東海村日本原子力研究所内）で複写による実費頒布をおこなっております。

JAERI-M reports are issued irregularly.
Inquiries about availability of the reports should be addressed to Information Division Department of Technical Information, Japan Atomic Energy Research Institute, Tokai-mura, Naka-gun, Ibaraki-ken 319-11, Japan.

編集兼発行　日本原子力研究所
印　　刷　いばらき印刷㈱

JAERI-M 92-173

Dynamic Behaviors of Fragments Ejected from the Surface of Carbon Materials by Laser Ablation

Osamu YODA, Atsumi MIYASHITA, Takasumi OHYANAGI*
and Kouichi MURAKAMI*

Department of Material Development
Takasaki Radiation Chemistry Research Establishment
Japan Atomic Energy Research Institute
Watanuki-cho, Takasaki-shi, Gunma-ken

(Received October 13, 1992)

A time-resolved X-ray absorption spectroscopy apparatus in the laboratory scale has been set-up by utilizing laser plasmas as an X-ray source. One of the major objectives using this apparatus is to observe X-ray absorption fine structures (XAFS) of various materials during materials processing in an energy region between 100eV and 3keV. For this purpose, we have provided two sets of optical and detecting systems. The most intense X-rays are generated from Au plasma and the intensity reaches as high as 10^{16} photons/pulse in 2π steradian in the energy region below 300eV. The energy resolution of the spectrometer $\Delta E/E$ has been determined to be 5×10^{-3}. The dynamic behavior of fragments ejected from the surface by laser ablation has been observed for a carbon rod and a pellet of C_{60} powder. Dominant fragments removed from the carbon rod have been found to be clusters, neutral atoms and ions. Maximum velocities of ejected clusters and atoms have been estimated to be less than 1.4×10^{4}m/s and more than 2×10^{4}m/s, respectively. C_{60} molecules have been removed from the pellet surface without decomposition by mild laser ablation. X-ray photoelectron measurements suggest that some reorganization has occurred on the surface of the ablated C_{60} pellet. A periodic structure has been discovered on the laser ablated C_{60} pellet and the spacing

---

* University of Tsukuba

of that periodic structure is explained by the surface scattering model.

Keywords: X-ray Absorption, Time-resolved, Laser Plasma, Materials Processing, Laser Ablation, Carbon, C_{60}, Polystyrene, Polymethylmethacrylate, X-ray Photoelectron Spectroscopy, Scanning Electron Microscopy, Binding Energy, Periodic Surface Structure, Surface Scattering Model

JAERI-M 92-173

レーザーアブレーションによって炭素系物質表面から飛び出したフラグメントの動的挙動

日本原子力研究所高崎研究所材料開発部
依田　修・宮下　敦巳
大柳　孝純*・村上　浩一*

(1992年10月13日受理)

レーザープラズマをX線源として用いた実験室規模時間分解X線吸収分光装置を作成した。この装置の使用主目的は，100eVから3keVのエネルギー範囲で，プロセス中の種々の物質のX線吸収微細構造を観測することである。金をターゲットに用いた時，300eV 以下のエネルギー範囲でもっとも強いX線が発生し，パルス当たり10^{16}光子の強度が得られた。分光器のエネルギー分解能は5×10^{-3}であった。この装置を用いて，炭素棒及びC_{60}粉末を圧縮したペレットをレーザーアブレーションしたときに表面から飛び出すフラグメントの動的挙動を観測した。フラグメントの主たる成分は炭素クラスター，中性炭素原子及び炭素イオンで，それらが表面から飛び出す速度はクラスターが1.4x10^4m/s以下，原子やイオンで2x10^4m/s以上と見積られた，弱いアブレーションではC_{60}分子がペレットから分解されずに飛び出す。光電子分光分析の結果からペレット表面の組織変化が示唆され，走査型電子顕微鏡による観察によって表面散乱モデルで説明できる周期構造が見い出された。

高崎研究所：〒370-12　群馬県高崎市綿貫町1233
＊筑波大学

Contents

目　　次

1. INTRODUCTION

The X-ray absorption spectroscopy near the absorption edges of a component element of materials is getting one of the most important tools to investigate the structure and property of materials. The fine structure near an absorption edge in the absorption spectrum, which is referred to as the near edge X-ray absorption fine structure (NEXAFS)‡, gives information on the electronic structure of the element, and an oscillating structure which appears at about 50 eV above an absorption edge, extended X-ray absorption fine structure (EXAFS) offers knowledge about the short range order around the absorbing element. These fine structures, the X-ray absorption fine structure, XAFS, can be observed commonly in the condensed system even if there is no long range order in matter. Hence, recently this technique is widely used for the analysis of amorphous states, liquids, solution, adsorbates on the surface as well as crystalline states. Furthermore, this method of analysis is well suited for the understanding of the process in thin film formation and materials processing by energetic beams such as laser and ions.

Thin films are formed by vacuum deposition, sputtering with ions or laser and chemical vapor deposition, and the nature of them depends on the fine structure, texture and the thickness of the film. Therefore, on one hand, it is important to analyze the structure of the deposited film itself in the static state. On the other hand, the understanding of dynamic processes during film formation and materials processing is indispensable to control quality of the film and to create new materials. For example, the state of fragments removed from the evaporation source affects much the nature and function of the film. The state may include species - whether the fragments are atoms, molecules or clusters, the electronic state - whether they are neutral or ionized, and the kinetic energy or the velocity of them.

For such studies as dynamic processes, the following features are required as an X-ray source of the absorption spectroscopy. 1) The source is of pulsed nature and the width of the pulse is sufficiently short corresponding to the time scale of changes in the atomic arrangement and/or electronic structures. 2) The energy distribution of the source is wide enough to cover various edges located separately in a broad energy range. 3) A smooth energy distribution is most desirable.

Synchrotron radiation (SR) satisfies above requirements and is very well suited for a light source of the X-ray absorption spectroscopy: the pulse width of SR is in the order of sub-nanoseconds and the smooth energy distribution of it covers from infrared to, depending on the electron energy in the storage ring, tens or hundreds keV. To access SR facilities is, however, sometimes difficult because of geographical and economic reasons. Beam lines are in general dedicated to many instruments and hence the machine time provided for each user is not always adequate. More essentially, the number of photons in a single SR pulse illuminating the sample

is often insufficient for the single shot measurement of an absorption spectrum: it requires many pulses to acquire meaningful data and this situation is disadvantageous for *in-situ* measurements during materials processing by pulsed radiation such as laser and ion beams.

Recently it becomes clear that hot and dense plasmas of high Z materials induced by high energy density laser irradiation emit pseudo-continuum soft X-rays. The application of these X-rays, laser plasma X-rays (LPX), has begun as an X-ray source of lithography[1]. LPX is also a promising X-ray source for XAFS measurements by the following favourable characteristics[2,3]. 1) The pulse width of LPX is as short as or shorter than that of the irradiated laser beam. 2) The energy distribution of emitted LPX and the conversion efficiency of the laser energy to X-rays depend on factors such as the electronic structure of target materials and the wavelength, the energy density and the pulse width of laser. By choosing an appropriate target material, one can obtain X-rays with nearly continuum energy distribution. 3) With the use of a laboratory scale laser system, the number of photons included in a single X-ray pulse is in many cases enough for the single shot measurement of an absorption spectrum in the specific energy region.

In the case of the laboratory scale set-up of a spectrometer using LPX, there is a limitation that utilizable X-rays have energies up to only a few keV. In this energy region, however, are included K-absorption edges of many important elements such as carbon, nitrogen, oxygen, aluminum and silicon, and L-edges up to medium Z elements. Therefore, LPX is quite an attractive X-ray source for the dynamic investigations of materials composed of light elements. If a laboratory scale laser system of nanosecond or shorter in pulse width is available, one could set-up a laboratory scale time-resolved X-ray absorption spectroscopy apparatus with sufficient temporal resolution for the study of dynamic processes, which is not feasible by use of SR at the moment.

Based on the above considerations, we have most recently set up a nanosecond time-resolved X-ray absorption spectrometer using LPX. This apparatus is designed to observe XAFS in energies ranging from 90eV to 3keV[4] and is used to investigate structural and electrical changes during materials processing by energetic beams[5]. At present, there are only a few X-ray absorption spectrometers in the world using LPX as an X-ray source[6,7]. Among them, our apparatus is the only one operating laboratory scale spectrometer in the world for *in-situ* measurements during materials processing.

In the present paper, we report briefly the outline of our laboratory scale apparatus for the nanosecond time-resolved XAFS measurement and demonstrate new results so far obtained by using this apparatus along with some other related topics disclosed through laser ablation of C_{60}.

2. OUTLINE AND CHARACTERISTICS OF THE APPARATUS

Our apparatus is composed mainly of three parts: the laser system, the spectrometer and the data acquisition system. The spectrometer is constituted by three vacuum chambers with vacuum systems: the target chamber in which X-rays are generated and emitted X-rays are collected by toroidal mirrors as an X-ray source of XAFS measurements, the sample chamber in which the sample is installed and the analyzing chamber in which the energy of probing and absorbed X-rays are analyzed. A computer is provided both for the data acquisition and for the regulation and adjustments for samples and optical systems. Figure 1 shows a schematic diagram of the apparatus and Fig. 2 shows the outlook of the spectrometer by a photograph.

2.1 Laser system

Two 12ns pulsed laser beams of 532nm, 7J and 1J in energy, are used to generate X-rays and to irradiate samples, respectively, which are provided by passing a 20J Nd:YAG/glass laser (Continuum K.K.) beam through second harmonics generators (SHGs). The pulse width of the laser is about 11ns. A delay circuit is installed in the 7J beam path to adjust the timing between sample irradiation and probing.

2.2 Spectrometer

2.2.1 Target chamber

The 7J beam is focused on a cylindrical target by a lens, 400mm in focal length, to produce hot plasma and hence X-rays in the target. The maximum laser irradiance is about 1 x 10^{13}W/cm^2. The target rod, 40mm in diameter, moves helicaly to expose a fresh surface for every laser shot. As mentioned earlier, we will observe XAFS in rather wide energy range. For this purpose, we use two sets of optical systems, i.e., two collection mirrors, two polychromators and two detectors, to cover the entire energy region of 90eV-3keV. Generated X-rays are collected by two toroidal mirrors with their surface normals arranged perpendicular to each other and to the probing direction of X-rays; one is for lower energy X-rays (90-1000eV) and the other for higher energy ones (1-3keV), which are set at 30 degree with respect to the incident laser beam. The solid angles subtended by two mirrors are 6.7×10^{-5} and 8.5×10^{-5}sr for lower and higher energy X-rays, respectively. Smooth and maximum efficiencies of the mirror reflectivity are achieved by coating platinum for lower energy X-rays and palladium for higher energy ones.

The yield and the pulse shape of X-rays are monitored by a 7 channel X-ray diode (XRD; KMS Fusion, Inc.) with filters of various energy pass bands and a digital oscilloscope (OSC; Tektronix). To measure the angular distribution of the X-ray yield, XRD can be attached to franges located at every 15° from 30 to 105 degrees with respect to the incident laser beam. In

Fig. 3 is shown the inner part of the target chamber in which we can see a focusing lens, a stack of metal targets and two collecting toroidal mirrors.

2.2.2 Sample chamber

X-rays are focused at the position of the sample and then incident on the energy analyzers. The 1 J beam is introduced into the sample chamber through a lens and irradiates samples with an effective maximum energy density of about 150J/cm^2 by adjusting the position of the lens. Samples can be also irradiated by high energy heavy ions from a cyclotron through a duct attached to the sample chamber. For the investigation of the surface of bulk samples, reflection experiments can be performed with the use of two flat Ni-coated reflection mirrors inserted up and down streams of the sample, in addition to standard transmission measurements.

2.2.3 Analyzing chamber and data acquisition system

A grazing incidence flat-field grating with 2400 lines/mm (Hitachi Ltd.) is used to analyze X-rays below 1000eV and a convex curved KAP crystal (001; 2d = 2.66nm) is utilized as a polychromator for higher energy X-rays. The detection of X-rays is made by two 1024 channel MCP/diode-array systems (Hamamatsu Photonics, Ltd.) for both energy regions. Controls and adjustments of the target, samples, optics and detectors, and data acquisitions are all carried out with an HP9000-345C+ computer. For a more detailed description of the apparatus, see Reference 8.

2.3 X-ray Intensity

The pulse shape and the X-ray yield have been measured by XRD with a polycarbonate filter, 0.5μm thick, which has almost flat X-ray sensitivity between 100 and 300eV. Figure 4 shows pulse shapes of laser and X-rays. The full width at half maximum of the X-ray pulse is about 11ns irrespective of the target material, which is narrower than that of the laser pulse by about 10 %. The X-ray yield has been examined on various metal targets. Among them, Au has emitted the most intense X-rays in the above energy region.

Because the angular distribution of the X-ray yield has behaved like a cosine function, the X-ray emission can be assumed to be isotropic in 2π steradian. Based on this, the total X-ray intensity of Au is estimated to be 1×10^{16}photons/pulse in 2π steradian and the maximum conversion efficiency of the laser energy to X-rays to be 4.6%. The number of photons illuminating the sample is evaluated to be 1.8×10^{11}/pulse by taking into account of the solid angle and the reflectivity of the collection toroidal mirror.

2.4 Source X-ray spectra

Figure 5 shows the source X-ray spectra of Al and Au in the lower energy region, and of Cu and Hf in the higher energy region obtained by a single laser shot with a laser irradiance of $1x10^{13}$ W/cm^2. In general, X-rays from low Z materials contain a lot of sharp line radiation whereas those from high Z materials exhibit rather continuum energy distributions; the former is utilized for the energy calibration and the determination of the energy resolution ($\Delta E/E$) of the spectrometer, and the latter is suited for the source of XAFS measurements.

For the energy calibration and the determination of the energy resolution of the spectrometer, a simulation spectrum has been synthesized by superimposing Gaussian broadened transition lines of a given target material in various ionization states[9] with the width of the broadening function as a resolution parameter. Such a simulation spectrum has been compared with the observed one from the same material and made best fit by changing the resolution parameter[8]. The energy calibration has been made satisfactorily and $\Delta E/E$ is found to be about $5x10^{-3}$. Table 1 summarizes typical source X-ray characteristics of our apparatus.

3. DYNAMIC BEHAVIORS OF FRAGMENTS REMOVED FROM THE SURFACE OF CARBON MATERIALS BY LASER ABLATION

Recently laser ablation is recognized to be well suited for formation of new materials such as carbon clusters[10] and high T_c superconducting thin films[11]. However, little is known about the formation mechanism of such materials. The dynamic analysis of ablation products, i.e., fragments removed from the surface of the source material by pulsed laser irradiation, is quite important in the sense that it gives a better understanding of the mechanism of materials formation as mentioned earlier in the introduction. We have started our experiments on the laser ablation of the substances containing group IV elements such as carbon and silicon. Here we show results concerning dynamic behaviors of carbon fragments removed from the sample surface by laser ablation through time-resolved measurements using our newly developed apparatus. This is probably the first attempt to observe fragments of carbon ejected from the sample surface by laser ablation with a temporal resolution of 10ns.

3.1 NEXAFS of foil samples in the vicinity of carbon K-edge

Before doing dynamic experiments, we have observed absorption spectra of foil samples in the vicinity of C K-edge as references by the standard transmission mode.

3.1.1 Experimental

Samples: Foil samples examined here are a carbon foil (Arizona Carbon Foil Co.) and polymer films of polystyrene (PS; -$CH_2CH\Phi$-) and polymethylmethacrylate (PMMA; -$CH_2C(CH_3)CO_2CH_3$-) with Φ being the phenyl group. The carbon foil, 10μg/cm^2 thick, is non-crystalline, which has been ascertained by electron and X-ray diffraction. Polymer films have been formed by casting drops of polymer dilute solution on water. Thickness of polymer films is between 0.1 and 0.2μm, which has been evaluated by absorption of X-rays.

Measurements: A gold target has been used for the generation of source X-rays with a laser irradiance of about 8 x 10^{12}W/cm^2. The duty cycle of the laser shot is 2/3 ppm. Five alternate measurements with and without samples have been done for absorbed and incident X-ray intensities. The fluctuation of the source X-ray intensity caused by the pulse-to-pulse variation of the laser power has been eliminated by monitoring the laser energy.

3.1.2 Results and discussion

Figure 6 shows absorption $\ln(I_0/I)$ of the samples. Here I_0 and I are the intensities of incident and transmitted X-rays, respectively. The spectrum of the carbon foil (Fig. 6a) consists of a sharp peak at around 285eV followed by broad absorption, the maximum of which lies around 295eV. The spectrum of PS (Fig. 6b) shows intense sharp peaks at 285 and

288eV, and that of PMMA (Fig. 6c) exhibits a shoulder at about 285eV and a sharp peak at 288eV.

The peak at around 285eV is characteristic for excitation of carbon 1*s* core electrons to π* antibonding orbitals in molecules containing π electrons[12]. Non-crystalline carbon and PS have many π electrons due to sp^2 hybridization and hence the peak intensity at 285eV is high in these materials while that in PMMA is weak because PMMA does not contain aromatic groups in its structure. The broad maximum between 290 and 310eV in non-crystalline carbon is assigned to transitions of 1*s* electrons to σ* antibonding bands which can be observed just above the ionization threshold[13]. The sharp peak at around 288eV appeared in PS and PMMA can be assigned to the C-H resonance or the Rydberg transition which is expected in saturated hydrocarbons[14], and is comparable with an energy of 288.0eV found for the excitation C1*s*→3*p* in methane and ethane[12]. The intense absorption above 290eV in PS and PMMA may be due to the transitions to σ* antibonding bands.

3.2 Spatial distribution of ablation products

3.2.1 Experimental

Materials: For the observation of ablation products, a carbon rod for vacuum deposition (purity: 99.9999%) and pure C_{60} (Texas Fullerenes Co., purity: better than 99.9%) have been irradiated by laser. C_{60} powder has been compressed into a thin pellet, 0.1mm thick and 13mm in diameter.

Laser irradiation and measurements: The laser intensity on the sample has been changed ranging from about 0.5J/cm^2 to 5J/cm^2 by adjusting the lens. Carbon K absorption spectra can be measured with time delays of 40 ~ 100ns between irradiation and probing by the length of the light path for the X-ray generation. The spatial dependence of the absorption spectrum has been obtained by altering the height of the sample. Other experimental conditions have been set same as described in the preceding section.

3.2.2 Results and discussion

In Fig. 7 we show spatial dependence of NEXAFSs of ablation products from the carbon rod in the region of the C K edge. The energy density of the laser for ablation is about 5J/cm^2 and the delay time between laser irradiation and probing is 100ns. Distances of probing X-rays above the sample surface are indicated in the figure in μm.

Absorption is stronger as the probing position is closer to the surface, indicating that ablation products are dense near the surface. The spectra exhibit a peak with fine structures between 280 and 290eV, and an intense broad absorption beginning at about 300eV. The former can be thought to be the superposition of 1*s*→π* and Rydberg transitions of carbon clusters, atoms and ions, and the latter mainly to be σ* bands of clusters. As the probing

distance increases, viz., over 1400μm, only two distinct peaks are present at 284 and 288eV and absorption beyond 300eV decreases. These two peaks are assigned to transitions $1s \rightarrow 2p$ of neutral carbon atom CI and single-charged ion CII, respectively[15].

To get an insight in the absorbing species diminished with distance, the difference in the absorption curve is indicative in some cases. Figure 8 shows, for example, the difference of absorption curves observed at 800 and 1000μm above the sample surface. Needless to say, the amount of species present at 1000μm is not always the same as that at the position of 800μm. However, provided that the amount does not change remarkably in this distance scale, the difference between these two absorption curves is a qualitative measure of diminished species between these two distances. From Fig. 8, one can see that the disappeared absorption are: 1) two sharp lines at 281 and 283.5eV, and 2) absorption at around 286eV followed by an intense broad component beginning at about 290eV. The former two kinds of absorption, which are clearly seen in the absorption spectra of rather near positions from the surface (Fig. 7), are not fully assigned at the moment. On the other hand, the latter component, which is also detected clearly in the difference of the absorption spectra at 1000 and 1200μm but absent between 1400 and 1600μm, quite resembles the absorption of graphite[12]. Therefore, the peak observed at around 286eV and broad absorption beginning at 290eV in the difference spectrum can be assigned to $1s \rightarrow \pi^*$ and $1s \rightarrow \sigma^*$ transitions, respectively, of clusters. However, the peak of $1s \rightarrow \pi^*$ transitions is rather broad and shifts towards the higher energy side by about 1eV as compared with the spectrum of graphite. This is presumably because either that the quantity of species at 800μm is different from that at 1000μm or that there exist clusters in various sizes and shapes, or both. The following situation is concluded about the spatial distribution of the species and the velocity of fragments. 1) Dominant fragments of ablated carbon are neutral atoms, ions and clusters in the region of 1200μm above the sample surface. 2) Because clusters cannot be observed over 1400μm, the velocity of clusters is estimated to be less than 1.4×10^4m/s. 3) Neutral carbon atoms and ions which have not contributed to formation of clusters are detected beyond 1400μm above the surface and their maximum velocities exceed 2×10^4m/s.

Figure 9 shows absorption spectra of fragments ablated from the C_{60} pellet. The energy densities of laser on the sample are (a) <0.5J/cm^2 and (b) 5J/cm^2. In the figure, the probing position of the topmost curve is very close to the sample surface and, from top to bottom, measurements have been done at every 200μm above the surface. The delay time between sample irradiation and probing has been maintained constant (100ns).

At lower irradiation energy density (Fig. 9a), two peaks at 284.5 and 286eV and a shoulder at around 287eV are seen below 290eV in photon energy. The energy density in this case is slightly above the ablation threshold observable by our apparatus. Peak positions and their intensities are essentially in good agreement with those obtained by high resolution

measurements[16] and also with those calculated by Hückel method[17] on C_{60}. These peaks are assigned to transitions of 1*s* core electrons to π^* antibonding molecular orbitals of the C_{60} molecule[16,17]. Figure 10 shows the difference between the absorption spectra obtained at 200 and 400μm above the surface. The shape of this difference spectrum is almost identical to the original absorption spectra. This fact implies that the species absorbing X-rays at 200 and 400μm are the same and only the quantity of fragments decreases as the probing position leaves from the surface. It is, therefore, concluded that C_{60} molecules are removed from the pellet surface without decomposition by mild laser ablation. Because the absorption spectrum of C_{60} exhibits molecular features[16], it is not distinguished whether ejected molecules are isolated ones or molecular aggregates.

At higher irradiation energy density (Fig. 9b), the shapes of absorption spectra are quite similar to those of fragments ablated from the carbon rod (cf. Fig 7), though the spatial distribution is to some extent confined near the surface in this case. This indicates that the energy density of laser is so high that C_{60} has decomposed into small clusters, neutral atoms and presumably ions of various ionization states.

4. THE SURFACE STRUCTURE OF C_{60} AFTER LASER ABLATION

The surface structure of C_{60} after laser irradiation has been examined by X-ray photoelectron spectroscopy (XPS) and scanning electron microscopy (SEM).

Since the discovery[10] and the establishment of the synthetic method[18] of C_{60}, investigations of fundamental properties as well as the possibility of industrial applications of it has been carried out quite extensively. C_{60} is a molecule which is composed of sixty carbon atoms with twenty six-membered and twelve five-membered rings, a truncated icosahedron, and is sometimes refereed to as a fullerene or a soccerball. The synthesized C_{60} powder is crystalline with the face-centered-cubic (FCC) crystal lattice. Solid C_{60} is an insulator with an electron bandgap of 1.5eV[19], but doping of, for example, potassium, even superconductivity emerges[20]. Much more interesting features on C_{60} will be disclosed hereafter.

C_{60} is the third crystalline form of pure carbon, completely different from other crystalline forms of carbon - diamond and graphite. It is quite interesting to know how this kind of molecules is formed by laser ablation[10], which is not known at present. With a view to understanding the formation mechanism, it is necessary to make clear the dynamic process during laser ablation of carbon. The following investigations are a part of our attempts to contribute to the understanding of the formation mechanism of C_{60}.

4.1 Experimental

Before laser ablation, as-compressed C_{60} pellet, which is hereafter referred to as original pellet, has been examined by XPS. After ablation experiments, the pellet, with a part of it being ablated, has been mounted on a sample holder with silver paste in air and XPS spectra have been observed for laser ablated and non-ablated portions on the pellet. The pellet has then been coated with gold and examined by SEM.

The surface chemical structure has been studied by a VG ESCALAB-200 spectrometer with MgKα X-rays (1253.6eV) for excitation. This instrument has been operated with a base pressure of 3×10^{-10} Torr. The energy calibration of the spectrometer has been carried out with the use of the binding energy of the metallic gold $4f_{7/2}$ line which is expected to appear at 83.9eV. The charging effect of the sample has been corrected by using O1*s* binding energy of adsorbed oxygen on the (0001) plane of highly oriented pyrolitic graphite (Union Carbide Corp.) appeared at 532.2eV as a standard. Through all XPS measurements, no special efforts have been made for cleaning the surface of the pellet and graphite.

The surface morphology has been investigated on the same parts of the pellet examined by XPS. The scanning electron microscope (JEOL 733) has been operated with an accelerating voltage of 15kV.

4.2 Results and discussion

4.2.1 Surface chemical structure

Figure 11 shows C1*s* spectra of the original pellet, ablated and non-ablated portions on the pellet. Table 2 summarizes C1*s* binding energies of them along with the C1*s* binding energy of graphite as a reference. The table also shows the peak intensity ratio of O1*s* and C1*s* lines in the wide scan spectrum for each sample, which provides important information on the elemental composition near the surface.

From Table 2 and by comparing these three figures, one can see the following features. 1) *Binding energy*: The binding energies of the original pellet and graphite as well as the non-ablated portion are identical within the experimental error to be 284.1eV. A slight shift, viz. -0.3eV in binding energy, is detected for the ablated portion. 2) *Original C_{60} pellet* (Fig. 11a): the C1*s* line is broadened towards higher binding energy side to a large extent as compared with that of graphite and a peak is clearly seen at the binding energy by 1.8eV higher than the main peak, which is followed by small structures. 2) *Ablated portion* (Fig. 11b): the line shape is symmetric and the line width is as narrow as that of graphite, and there exist weak wiggles in the higher binding energy side starting at 1.8eV from the main C1*s* peak. 3) *Graphite* (Fig. 11c): the C1*s* line is sharp but it tails towards higher binding energy side to some extent, which is attributed to the many-body effect on core ionization, or in other words, continuous shake-up-type events due to the existence of a distribution of the unfilled band above the Fermi level in graphite[21].

The C1*s* spectrum of the original pellet is in good agreement with the spectrum of C_{60} observed by Weaver *et al.*[22] except a large broadening towards higher binding energy side. The peak at about 286eV and the following small structures in the original pellet can be assigned to the shake-up satellites, $\pi\rightarrow\pi^*$ and $\pi\rightarrow\sigma^*$ transitions, respectively. The existence of $\pi\rightarrow\pi^*$ satellites is a proof of aromaticity[21]. The origin of large asymmetry in the C1*s* line shape in the original pellet cannot be attributed to transitions to the continuous unfilled levels which are the primal cause of asymmetry in the case of graphite, because C_{60} is an insulator. Rather, it should be attributed to roughness and inhomogeneity on the surface of the original C_{60} pellet[23].

By laser ablation, the C1*s* spectrum becomes sharp and symmetric, although small wiggles can still be seen beyond 286eV, which implies that roughness and inhomogeneity have been removed from the pellet surface. Furthermore, a great deal of desorption of oxygen has occurred near the surface of the C_{60} pellet, because the O1*s*/C1*s* ratio in the ablated portion decreases remarkably as compared with that in the original pellet (see Table 2). The above findings suggest that some reorganization has been introduced on the C_{60} pellet surface by laser ablation. One possible explanation of the desorption of oxygen and the removal of roughness from the surface layer is that the melt-recrystallization process has occurred on the ablated

surface which could lead to the growth of grains composed of C_{60} powder and hence reduction in oxygen once adsorbed on the grains and introduction of surface smoothness, although the melting behavior of the FCC C_{60} crystal under laser ablation circumstances is not clear at present. The structure of the ablated C_{60} surface is discussed in the next section.

4.2.2 Periodic surface structure by laser ablative etching

In Fig 12, the surface morphologies observed by SEM are shown for non-ablated and ablated portions on the C_{60} pellet surface. Laser has been irradiated for 13 shots with an energy density of <0.5J/cm^2 and at an angle of 45° to the normal on the pellet. At the non-ablated portion, C_{60} powder is compressed into grains and the pellet surface is rather rough. On repeated laser pulse irradiation, periodic surface structures or ripples have been discovered on the whole area of laser irradiation as shown in Fig. 12b.

Formation of periodic patterns by laser irradiation has been so far reported on metals, semiconductors and polymers with laser wavelengths ranging from infrared to ultraviolet[24,25]. Theoretical treatments have been also made for the formation mechanism of such periodic structures[24,26]. Among them, the surface scattering model is rather widely applied successfully[27]. According to the surface scattering model, for oblique incidence of *p*-polarized laser beam, the spacing of the ripple X is given by one or the other of the following equation[21].

$$X = \frac{\lambda}{1 \pm \sin\theta}, \qquad (1)$$

where λ and θ are the wavelength of laser and the angle of incidence from the normal to the surface. With λ = 532nm and θ = 45° , Xs in our case are calculated to be 312nm and 1.816μm for + and - signs in the denominator, respectively. From Fig. 12b, one can obtain the spacing of the periodic structure on the C_{60} pellet to be 320nm. This is in good agreement with Eq. (1) in the case that the + sign is applied. However, the mechanism of determining which spacing will appear is not known theoretically nor experimentally, and further investigations will be needed.

ACKNOWLEDGEMENTS

The authors wish to thank Profs. S. Aoki and N. Yamaguchi of University of Tsukuba, Drs. F. Bijkerk, G. van Dorssen and E. Louis of FOM Institute, The Netherlands, for valuable suggestions on the design of our apparatus. They are also indebted to Mr. H. Ito for the measurement of the scanning electron microscopy.

REFERENCES

‡ In recent years, the absorption near edge structure, or the Kronig structure, has been mostly referred to as the X-ray absorption near edge structure, XANES. However, here we use the term NEXAFS after Stöhr[28]. NEXAFS is mainly used for K-shell excitation spectra of low Z molecules in relation to the surface.

1) F. Bijkerk, E. Louis, G.E. van Dorssen and M.J. van der Wiel: SPIE **1089** (1989) 274.
2) D.J. Nagel: Adv. X-ray Anal. **18** (1975) 1.
3) H.C. Gerritsen, H. van Brug, F. Bijkerk and M.J. van der Wiel: J.Appl. Phys. **59** (1986) 2337.
4) A. Miyashita and O. Yoda: JAERI-M, **88-212** (1988).
5) K. Murakami, H.C. Gerritsen, H. van Brug, F. Bijkerk, F.W. Saris and M.J. van der Wiel: Phys. Rev. Lett. **56** (1986) 655.
6) H.M. Epstein, R.E. Schwelzel, P.J. Mallozzi and B.E. Campbell: J. Amer. Chem. Soc. **105** (1983) 1446.
7) R.W. Eason, D.K. Bradley and G.N. Greaves: J. Phys. C **17** (1984) 5067.
8) A. Miyashita, O. Yoda, K. Murakami, T. Ohyanagi, S. Aoki and N. Yamaguchi: Laser Adv. Mater. Process. **2** (1992) 1029.
9) R.L. Kelly: J. Phys. Chem. Ref. Data **16** (Suppl. 1) (1987).
10) H.W. Kroto, J.R. Heath, S.C. O'Brien, R.F. Curl and R.E. Smally: Nature **318** (1985) 162.
11) K. Murakami: Europ. Mater. Res. Soc. Monogr. **2** (1992) 125.
12) W. Eberhardt, R.P. Haelblich, M. Iwan, E.E. Koch and C. Kunz: Chem. Phys. Lett. **40** (1976) 180.
13) D. Arvanitis, K. Barbeschke, L. Wenzel and U. Dobler: Phys. Rev. Lett. **57** (1986) 3175.
14) G. Comelli, J. Stöhr, C.J. Robinson and W. Jark: Phys. Rev. B **38** (1988) 7511.
15) E. Jannitti, P. Nicolosi and G. Tondello: Physica Scripta **41** (1990) 458.
16) L.J. Terminello, D.K. Shuh, F.J. Himpsel, D.A. Lapiano-Smith, J. Stohr, D.S. Bethune and G. Meijer: Chem. Phys. Lett. **182** (1991) 491.

ACKNOWLEDGEMENTS

The authors wish to thank Profs. S. Aoki and N. Yamaguchi of University of Tsukuba, Drs. F. Bijkerk, G. van Dorssen and E. Louis of FOM Institute, The Netherlands, for valuable suggestions on the design of our apparatus. They are also indebted to Mr. H. Ito for the measurement of the scanning electron microscopy.

REFERENCES

‡ In recent years, the absorption near edge structure, or the Kronig structure, has been mostly referred to as the X-ray absorption near edge structure, XANES. However, here we use the term NEXAFS after Stöhr[28]. NEXAFS is mainly used for K-shell excitation spectra of low Z molecules in relation to the surface.

1) F. Bijkerk, E. Louis, G.E. van Dorssen and M.J. van der Wiel: SPIE **1089** (1989) 274.
2) D.J. Nagel: Adv. X-ray Anal. **18** (1975) 1.
3) H.C. Gerritsen, H. van Brug, F. Bijkerk and M.J. van der Wiel: J.Appl. Phys. **59** (1986) 2337.
4) A. Miyashita and O. Yoda: JAERI-M, **88-212** (1988).
5) K. Murakami, H.C. Gerritsen, H. van Brug, F. Bijkerk, F.W. Saris and M.J. van der Wiel: Phys. Rev. Lett. **56** (1986) 655.
6) H.M. Epstein, R.E. Schwelzel, P.J. Mallozzi and B.E. Campbell: J. Amer. Chem. Soc. **105** (1983) 1446.
7) R.W. Eason, D.K. Bradley and G.N. Greaves: J. Phys. C **17** (1984) 5067.
8) A. Miyashita, O. Yoda, K. Murakami, T. Ohyanagi, S. Aoki and N. Yamaguchi: Laser Adv. Mater. Process. **2** (1992) 1029.
9) R.L. Kelly: J. Phys. Chem. Ref. Data **16** (Suppl. 1) (1987).
10) H.W. Kroto, J.R. Heath, S.C. O'Brien, R.F. Curl and R.E. Smally: Nature **318** (1985) 162.
11) K. Murakami: Europ. Mater. Res. Soc. Monogr. **2** (1992) 125.
12) W. Eberhardt, R.P. Haelblich, M. Iwan, E.E. Koch and C. Kunz: Chem. Phys. Lett. **40** (1976) 180.
13) D. Arvanitis, K. Barbeschke, L. Wenzel and U. Dobler: Phys. Rev. Lett. **57** (1986) 3175.
14) G. Comelli, J. Stöhr, C.J. Robinson and W. Jark: Phys. Rev. B **38** (1988) 7511.
15) E. Jannitti, P. Nicolosi and G. Tondello: Physica Scripta **41** (1990) 458.
16) L.J. Terminello, D.K. Shuh, F.J. Himpsel, D.A. Lapiano-Smith, J. Stohr, D.S. Bethune and G. Meijer: Chem. Phys. Lett. **182** (1991) 491.

17) P.W. Fowler and J. Woolrich: Chem. Phys. Lett. **127** (1986) 78.
18) W. Krätschmer, L.D. Lamb, K. Fostiropoulos and D.R. Huffman: Nature **347** (1990) 354.
19) D.R. Huffman: Phys. Today November (1991) 22.
20) A.F. Hebard, M.J. Rosseinsky, R.C. Haddon, D.W. Murphy, S.H. Glarum, T.T.M. Palstra, A.P. Ramirez and A.R. Kortan: Nature **350** (1991) 600.
21) D. Briggs: in "Practical Surface Analysis" (John Wiley, Chichester UK, 1983) Chap. 3.
22) J.H. Weaver, J.L. Martins, T. Komeda, Y. Chen, T.R. Ohno, G.H. Kroll, N. Troullier, R.E. Haufler and R.E. Smalley: Phys. Rev. Lett. **66** (1991) 1741.
23) U. Gelius: private communication.
24) Z. Gousheng, P.M. Fauchet and A.E. Siegman: Phys. Rev. **B26** (1982) 5366.
25) H. Niino, M. Nakona, S. Nagano and A. Yabe: Appl. Phys. Lett. **55** (1989) 510.
26) J.E. Sipe, J.F. Young, J.S. Preddton and H.M. van Driel: Phys. Rev. **B27** (1983) 1141.
27) For example, P.E. Dyer and R.J. Farley: Appl. Phys. Lett. **57** (1990) 765.
28) J. Stöhr: "NEXAFS Spectroscopy" (Springer, New York, 1992).

Table 1 Typical source X-ray characteristics and the energy resolution of the spectrometer.

Target	: Gold	
Laser Irradiance	: 1 x 10^{13} W/cm^2	(12 ns FWHM)
Energy Range	: 100 ~ 300 eV	(0.5μm Polycarbonate Filter)
X-ray Pulse Width	: 11 ns	(FWHM)
X-ray Intensity	: 1 x 10^{16} photons/pulse	(2π steradian)
Conversion Efficiency	: 4.6 %	
Number of Photons at Sample	: 1.8 x 10^{11} /pulse	
Energy Resolution	: 5 x 10^{-3}	(ΔE/E)

Table 2 C1s binding energy and peak intensity ratio of O1s and C1s.

	As-compressed C_{60} Pellet	Ablated Portion of C_{60}	Non-ablated Portion of C_{60}	Graphite
C1s Binding Energy (eV)	284.14	283.84	284.14	284.08
Peak Intensity Ratio O1s/C1s	0.46	0.09	0.42	0.03

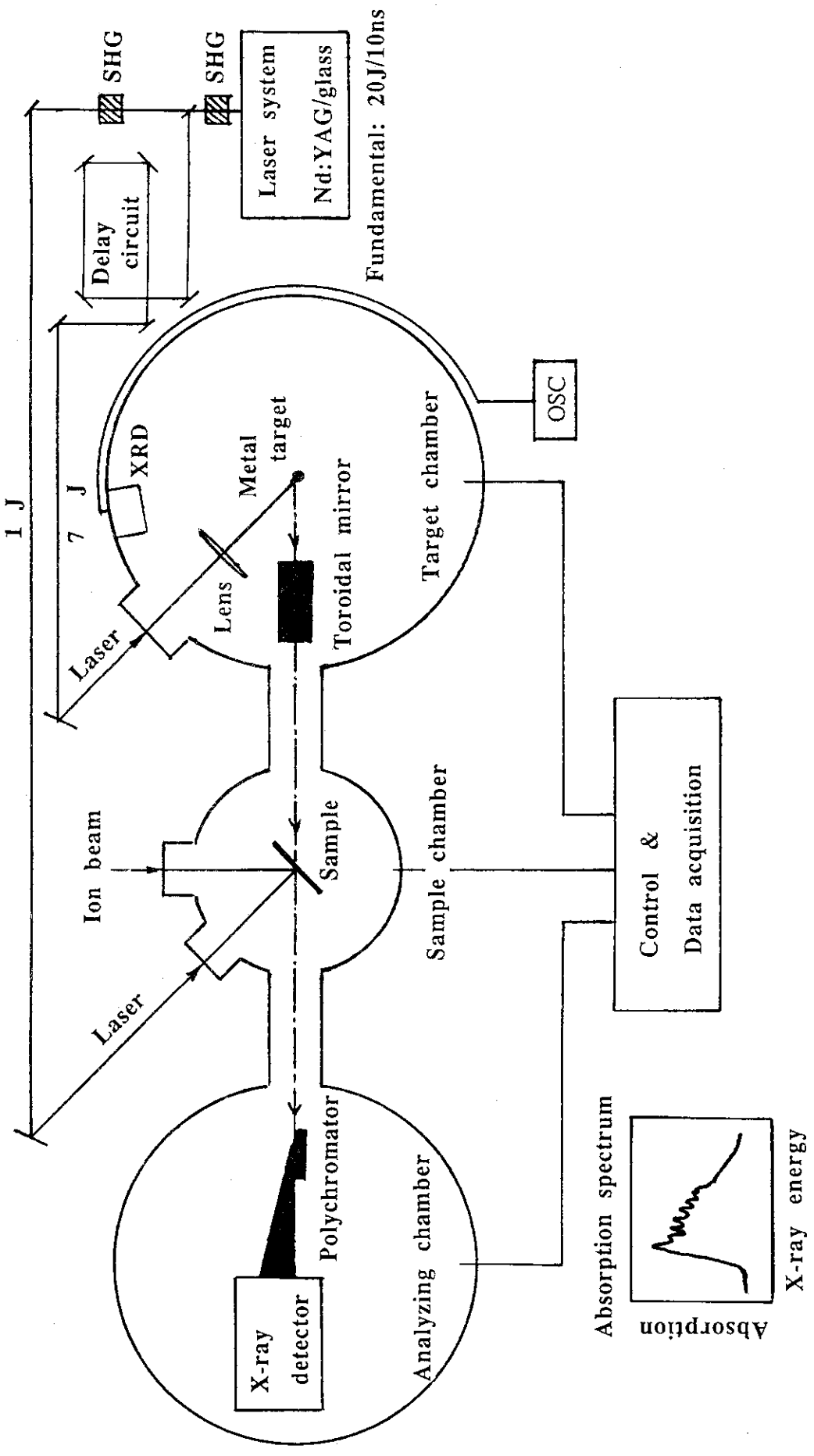

Fig. 1 Schematic diagram of the time-resolved X-ray absorption spectroscopy apparatus.

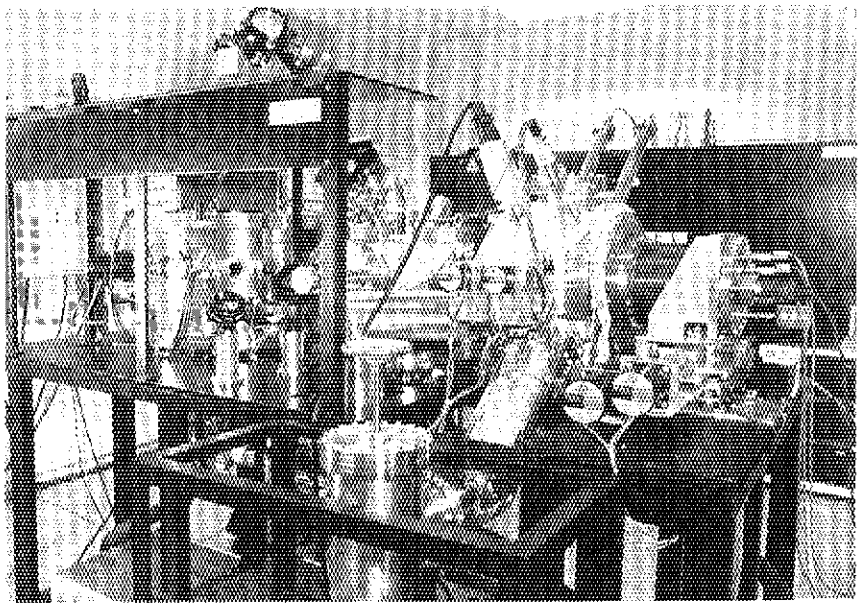

Fig. 2 Outlook of the time-resolved X-ray absorption spectroscopy apparatus. The spectrometer is on the front side and the laser system is in the black box on the rear side. Three vacuum chambers are, from left to right, the target, the sample and the analyzing chambers, respectively.

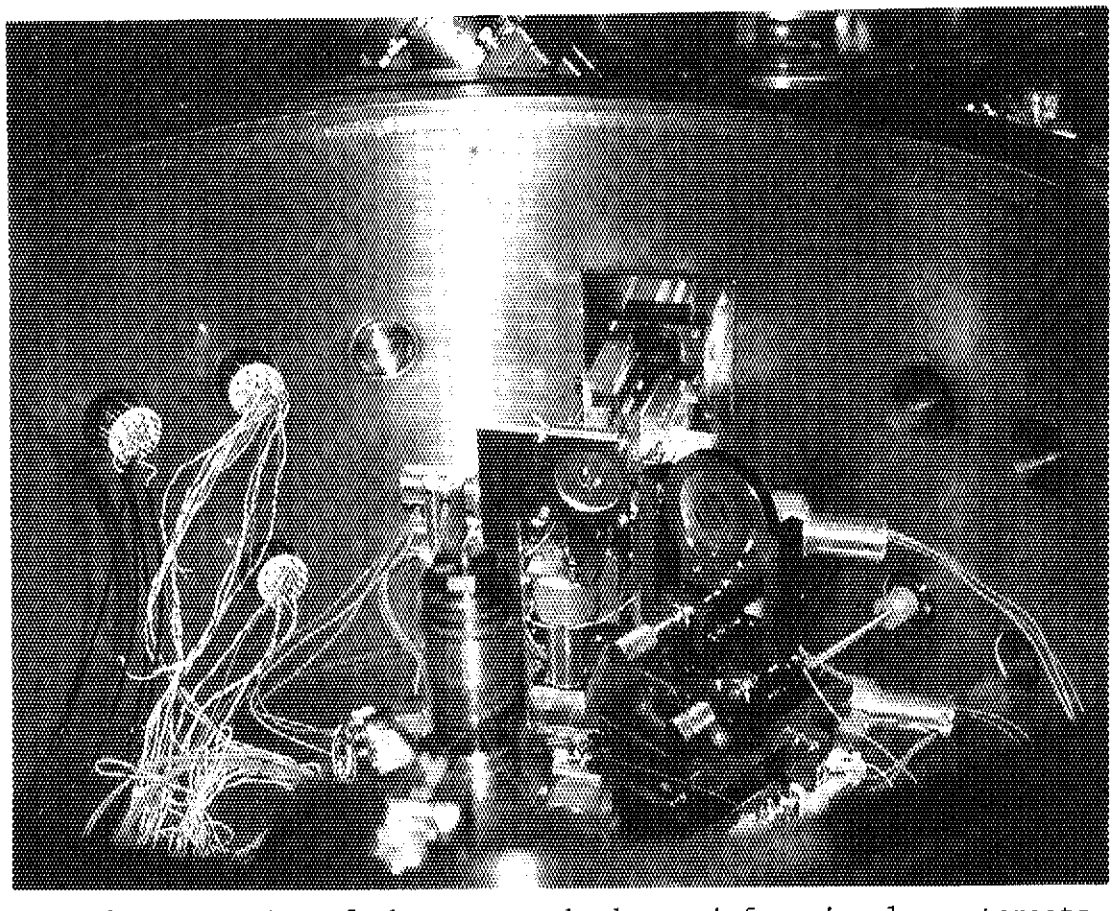

Fig. 3 Inner view of the target chamber. A focusing lens, targets, and two collection toroidal mirrors are seen.

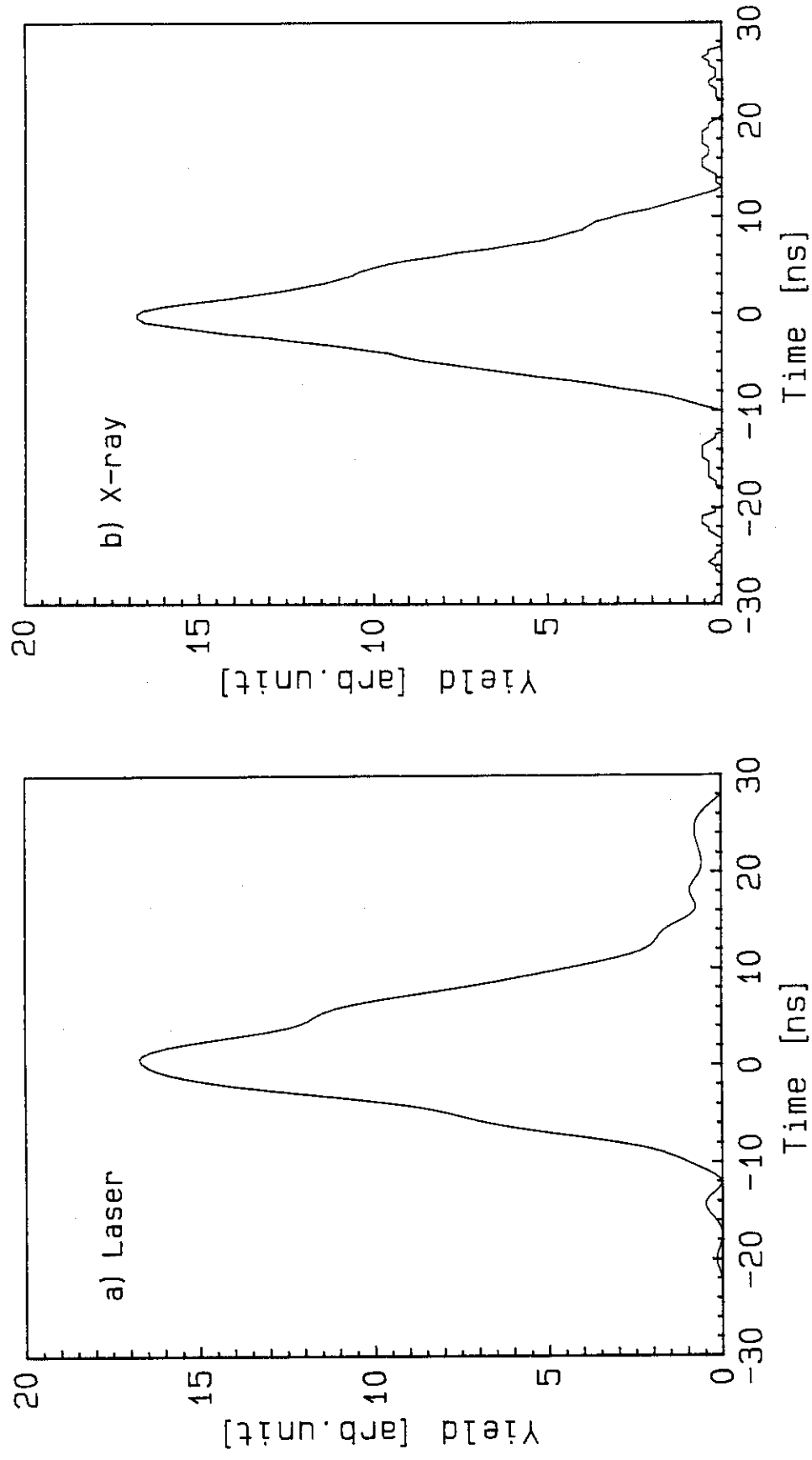

Fig. 4 Pulse shapes of a) laser and b) X-rays. The FWHM of the laser pulse is 12ns and that of X-rays is 11ns. The X-ray energy is between 100 and 300eV.

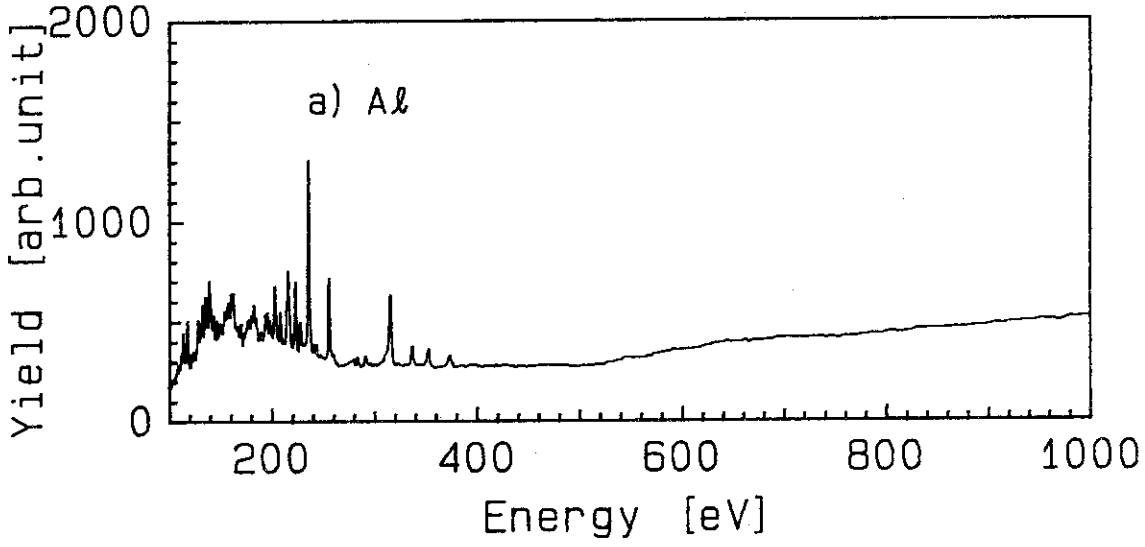

Fig. 5 Source X-ray spectra of a) aluminum and b) gold in 100 ~ 1000eV, and of c) copper and d) hafnium in 1 ~ 3keV.

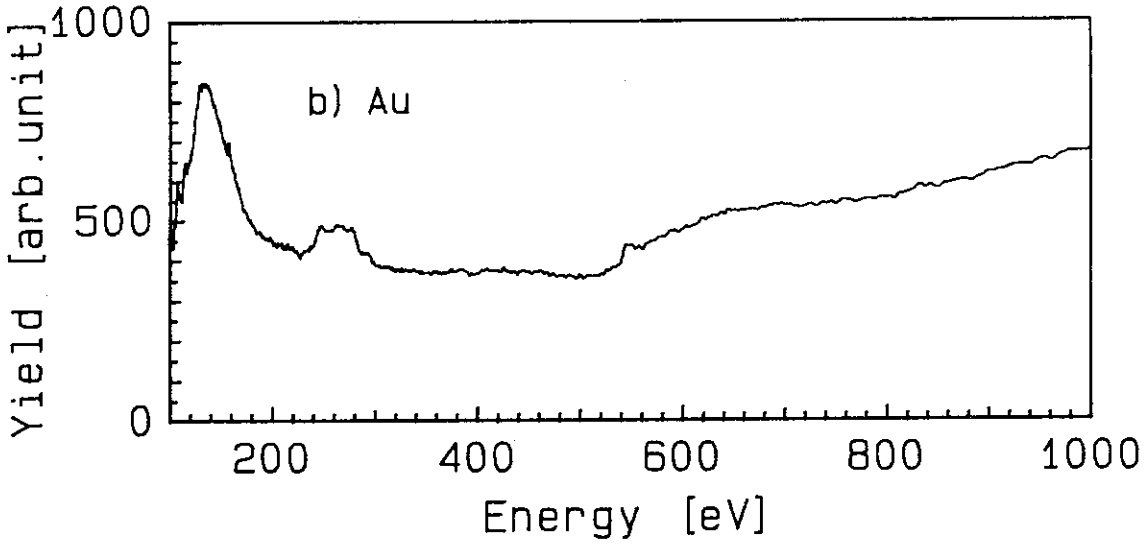

Fig. 5 (Continued) b).

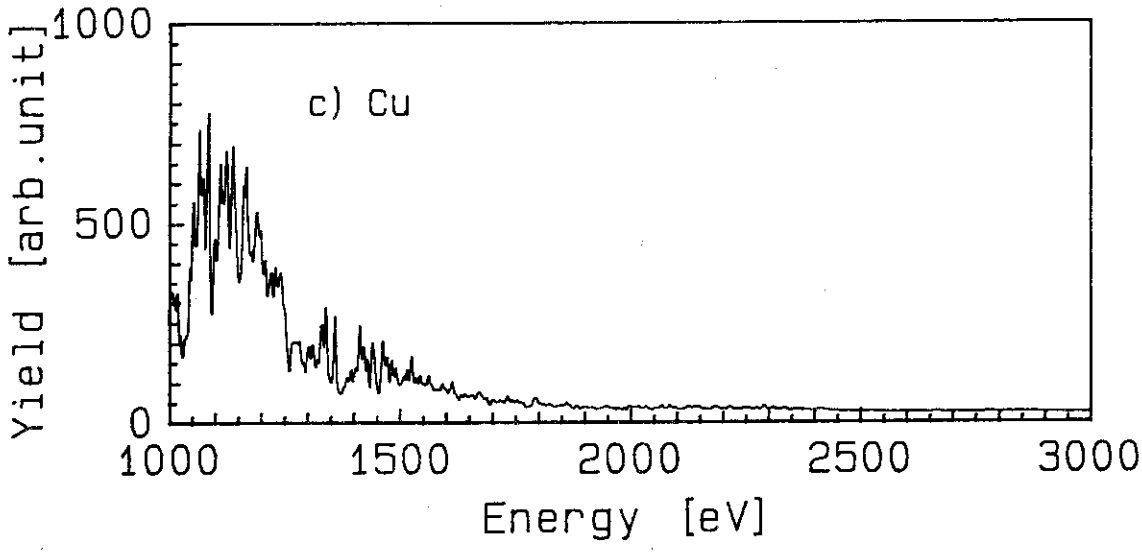

Fig. 5 (Continued) c).

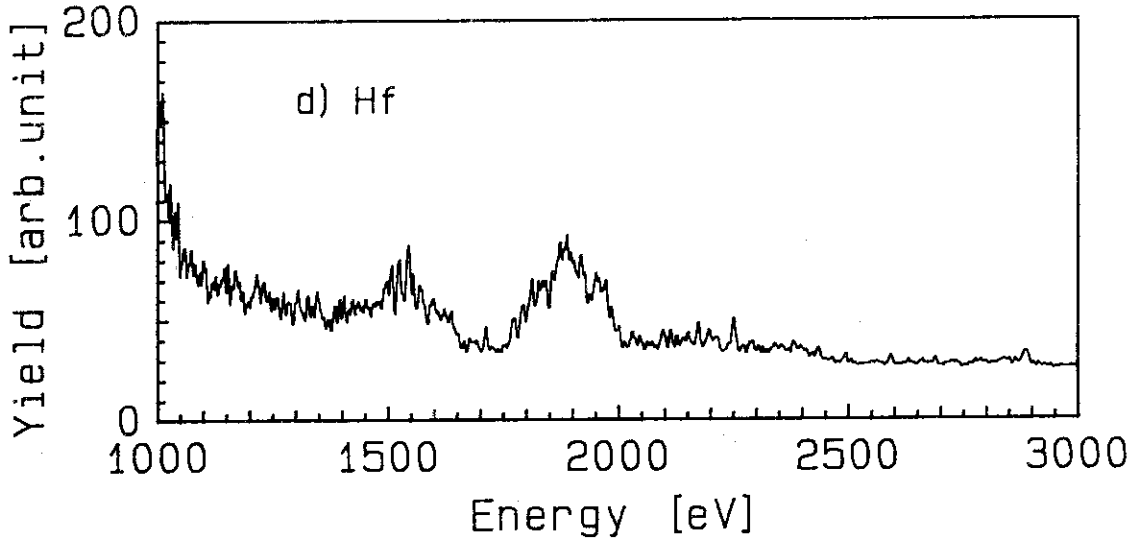

Fig. 5 (Continued) d).

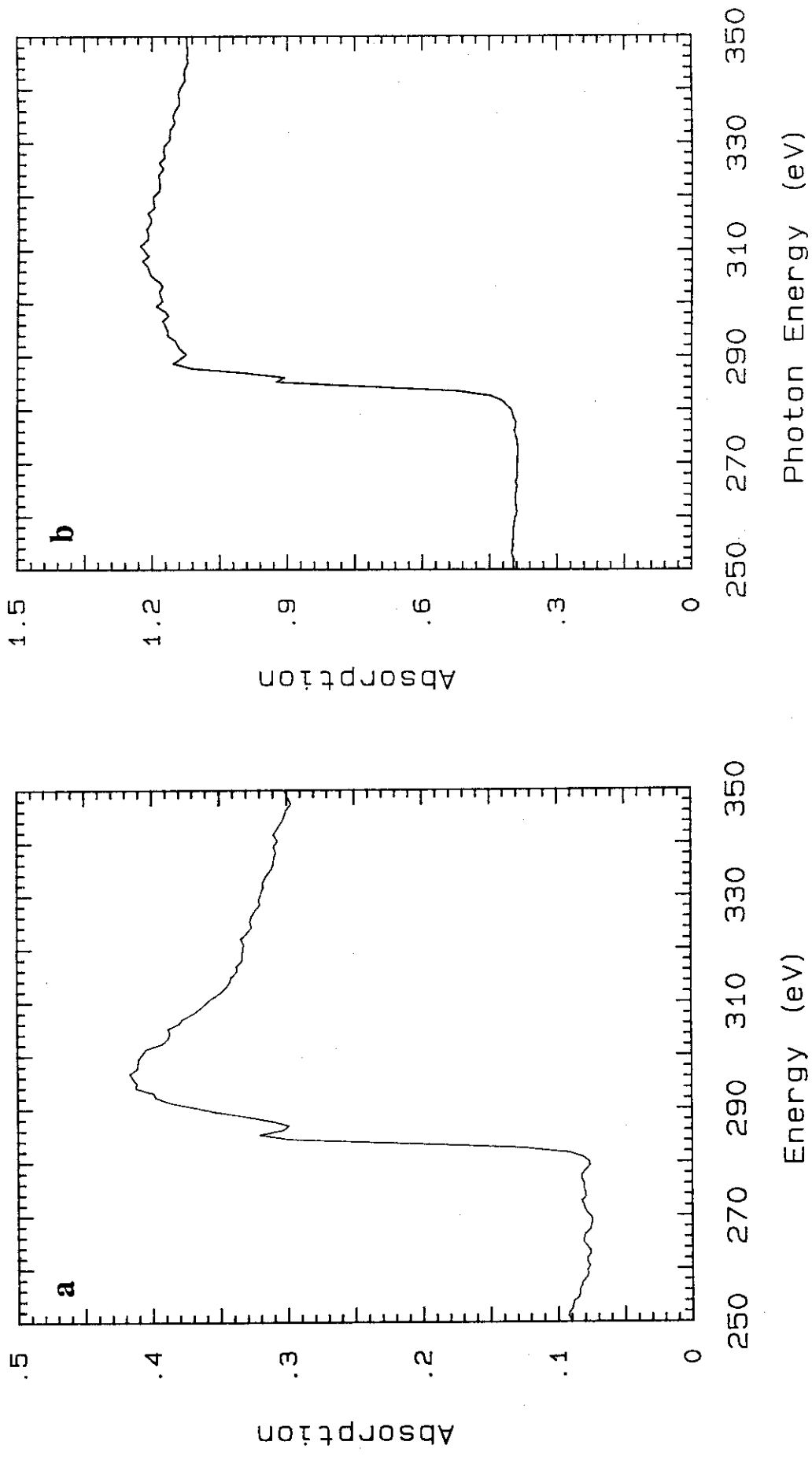

Fig. 6 Absorption spectra of a) non-crystalline carbon, b) polystyrene and c) polymethylmethacrylate foils in the vicinity of C K-edge.

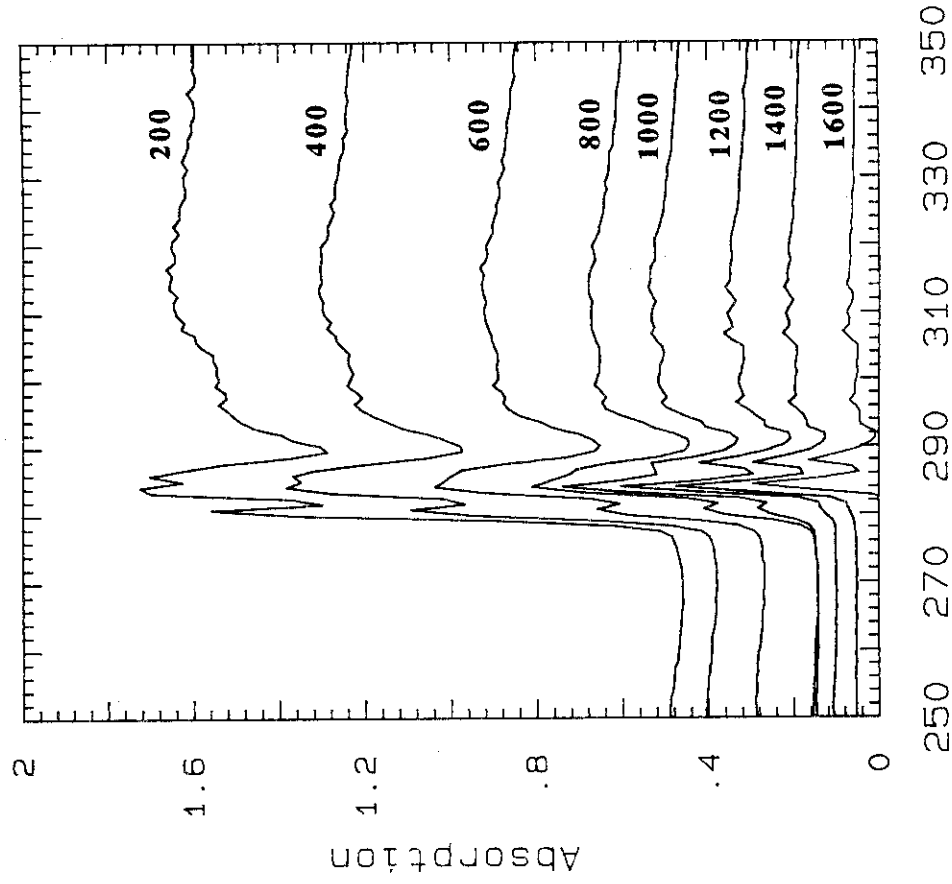

Fig. 7 Space dependent K absorption spectra of carbon vapor evaporated from solid carbon by laser irradiation. The delay time between laser irradiation and probing is 100ns, and the laser energy density is 5J/cm^2. Probing distances from the sample surface are indicated in the figure in μm.

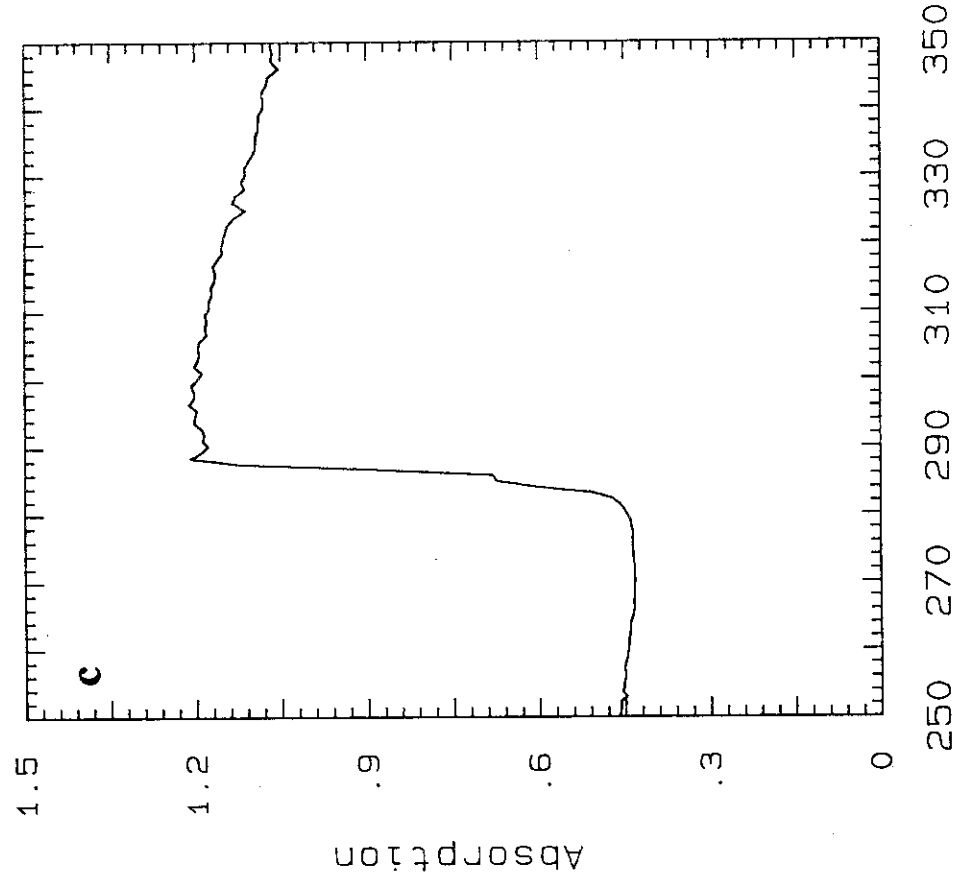

Fig. 6 (Continued) c).

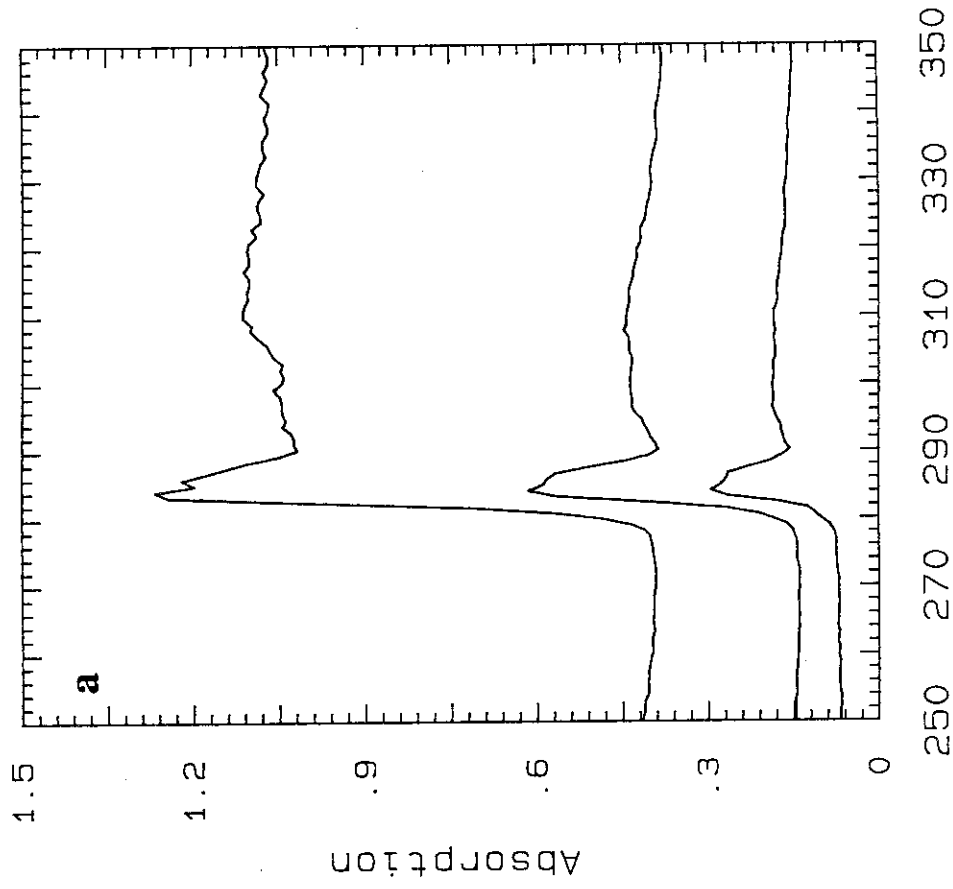

Fig. 9 Absorption spectra of fragments ablated from the surface of the C_{60} pellet. The energy densities of irradiation are a) <0.5J/cm^2 and 5J/cm^2.

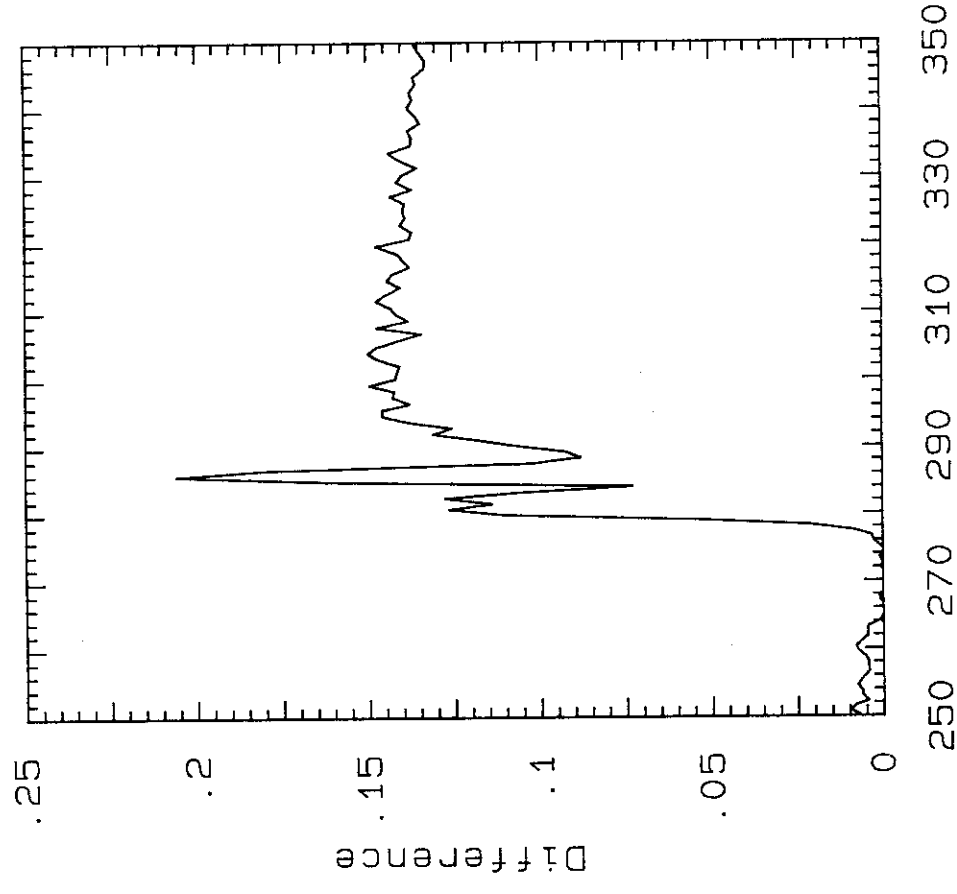

Fig. 8 Difference spectrum of the absorption spectra observed at 800 and 1000μm in Fig. 7.

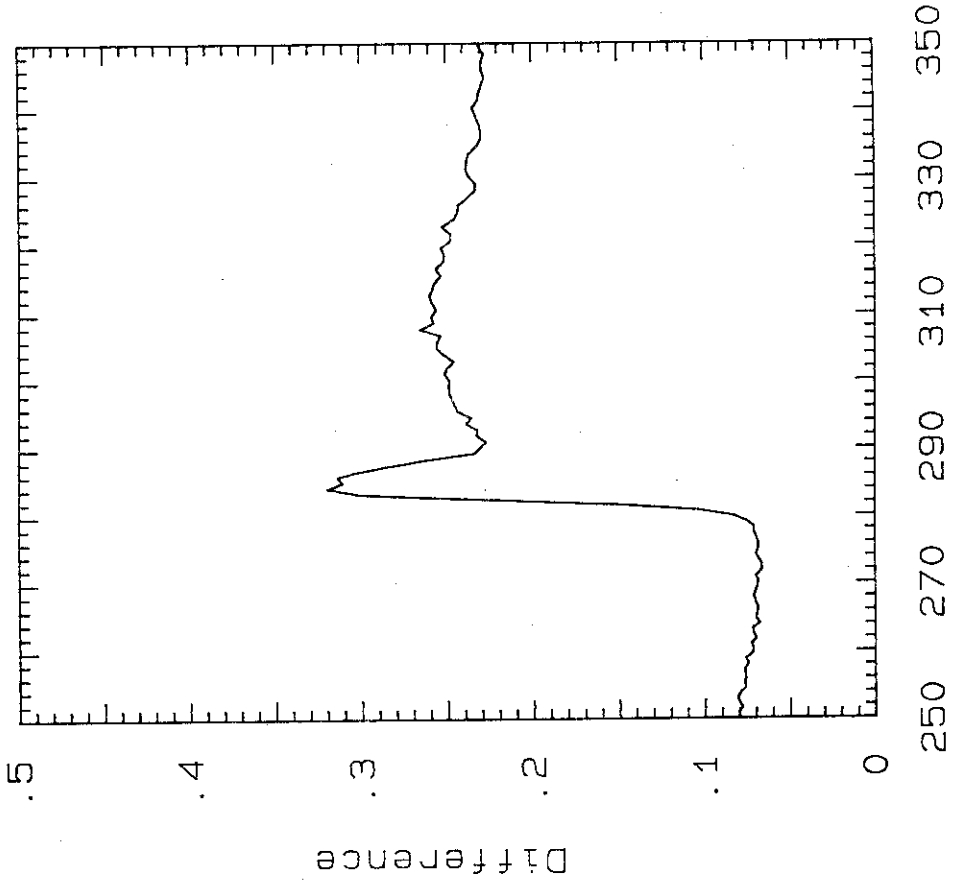

Fig. 10 Difference spectrum of the absorption spectra observed at 200 and 400μm in Fig. 9a).

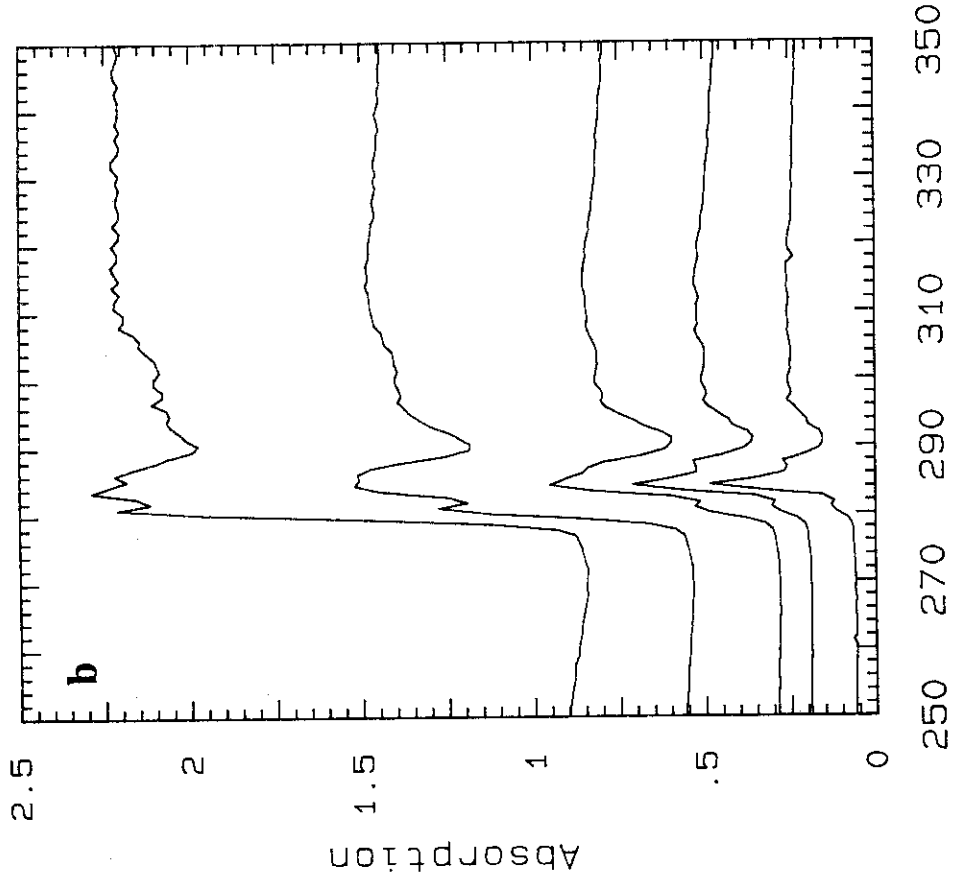

Fig. 9 (Continued) b).

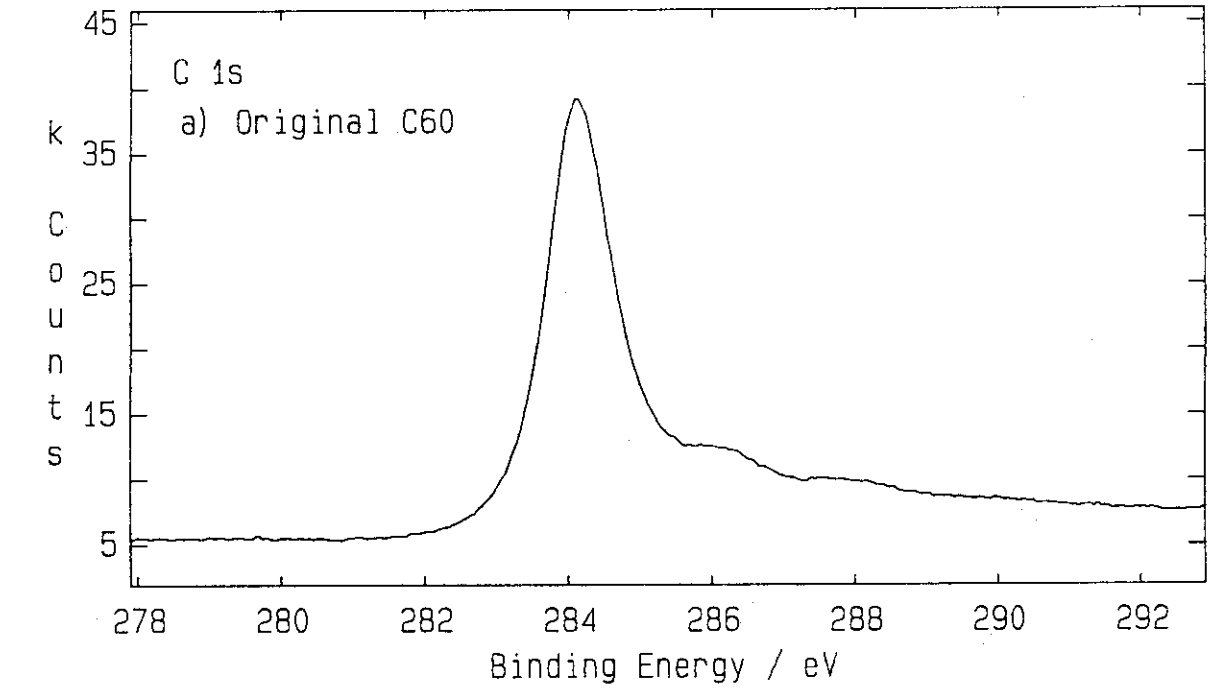

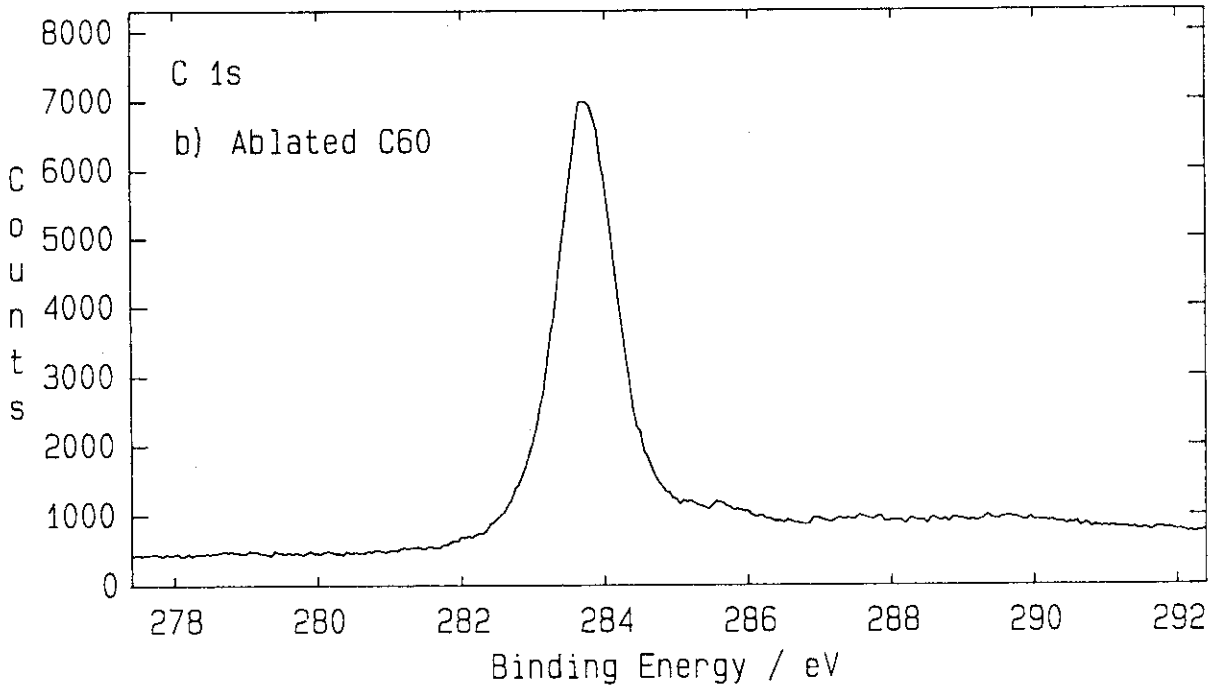

Fig. 11 XPS C1s spectra of a) original C_{60} pellet, b) ablated portion on the pellet and c) graphite.

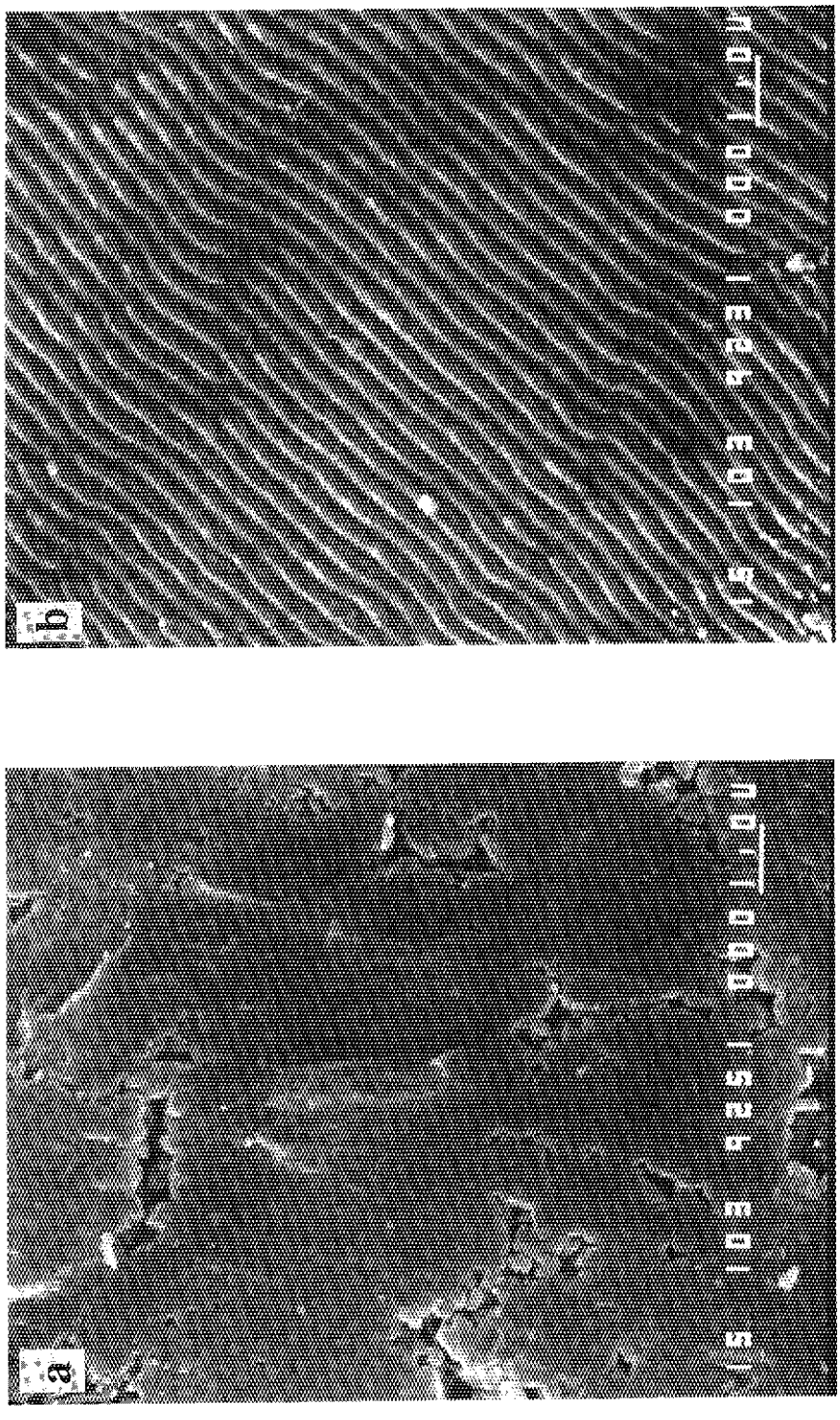

Fig. 12 SEM photographs of a) non-ablated and b) ablated portions on the C_{60} pellet.

JAERI-M
92-174

中性子照射に伴うベリリウム中のヘリウム生成量計算プログラム：HEINBE

１９９２年１１月

島川　聡司・石塚　悦男・斎藤　　実

日　本　原　子　力　研　究　所
Japan Atomic Energy Research Institute